Available online at www.sciencedirect.com
SCIENCE DIRECT®
Journal of Nuclear Materials 322 (2003) 228–234
journal of nuclear materials
www.elsevier.com/locate/jnucmat

Mechanical dispersion of Y_2O_3 nanoparticles in steel EUROFER 97: process and optimisation

V. de Castro [a,*], T. Leguey [a], M.A. Monge [a], A. Muñoz [a], R. Pareja [a], D.R. Amador [b], J.M. Torralba [b], M. Victoria [c]

[a] Departamento de Física, Universidad Carlos III de Madrid, Avd. de la Universidad 30, 28911 Leganés, Spain
[b] Departamento de Ciencia de Materiales, Universidad Carlos III de Madrid, Avd. de la Universidad 30, 28911 Leganés, Spain
[c] CRPP-EPFL Fusion Technology Materials, 5232 Villigen PSI, Switzerland

Received 16 May 2003; accepted 21 July 2003

Abstract

The procedures followed to produce Y_2O_3-dispersed EUROFER 97 powder ready to be compacted and hot isostatic pressing processed are reported. An attrition mill has been used under controlled conditions. The compositional and microstructural characterization of the Y_2O_3/EUROFER powder along the different steps of the milling process has allowed optimising the processing conditions to obtain a nanosized Y_2O_3 dispersion. TEM observations performed on Y_2O_3/EUROFER powder milled under these specific conditions reveal the presence of monoclinic Y_2O_3 dispersoids having sizes around 10 nm in the ferrite/martensite matrix.

1. Introduction

Environmental and safety regulations demand the use of low radiation-induced activation materials for the structural components of future fusion reactors. In addition, these materials have to be irradiation resistant and exhibit good mechanical properties and stability at elevated temperatures. Another major concern for the materials to be used in the blanket structure is their allowable maximum service temperature as it determines the overall efficiency of the reactor. Several reduced-activation Cr–W steels have been developed for structural applications in US, Japan and Europe [1–7]. Presently, the upper operating temperature for the reduced-activation ferritic/martensitic (RAFM) steels being considered for structural applications in future fusion reactors is established at 550 °C. One way to raise this temperature in RAFM steels up to around 650 °C is to reinforce them with a homogeneous dispersion of hard particles. Oxide dispersion strengthening operates in steels efficiently when a high density of nanosized particles, such as Y_2O_3 or TiO_2, is dispersed in the ferrite matrix [8–13]. It has been demonstrated that oxide-dispersion strengthened (ODS) ferritic steels can maintain good mechanical properties at elevated temperatures and have more swelling resistance than the austenitic steels.

Since no RAFM ODS steels are commercially available at present, the European Fusion Programme has considered initiating appropriate research activities to produce and characterize these materials in order to demonstrate the feasibility of their use in the blanket designs. The European reference RAFM steel EUROFER 97 has been chosen to be ODS with Y_2O_3 particles. Different batches of ODS EUROFER were prepared by mechanical dispersion and hot isostatic pressing (HIP) procedures at CEA (France) and Plansee (Austria) [14–16]. The processing details of these batches have not been reported. The tensile tests performed on Plansee batches with 0.3 wt%Y_2O_3 at Karlsruhe [15] and Villigen [16] indicate a strength increase of about 50% compared

* Corresponding author. Tel.: +34-91 624 94 12/91 84; fax: +34-91 624 87 49.
E-mail address: mvcastro@fis.uc3m.es (V. de Castro).

0022-3115/$ - see front matter © 2003 Elsevier B.V. All rights reserved.
doi:10.1016/S0022-3115(03)00330-1

to the strength of the basic steel EUROFER 97 and reasonable good mechanical characteristics at elevated temperatures. The results for the 0.5 wt%Y_2O_3 batches differ significantly. The discrepancies may be attributed to the presence of micropores in the hipped batches. The impact tests on the 0.3 wt%Y_2O_3 material result in maximum absorbed energy values remarkably lower than those for basic EUROFER showing an increase of the ductile-to-brittle transition temperature of about 200 degrees. The microstructural characterization of the ODS steels by transmission electron microscopy (TEM) has confirmed the presence of nanosized Y_2O_3 particles bimodally dispersed and the absence of the characteristic martensite laths in as-hipped samples [15,16].

The lack of precise processing details has not allowed establishing any relationship between the milling processes, the microstructure and mechanical properties of these ODS steels and precludes attempts to improve their mechanical characteristics by the control of the milling process. The correct control processing of the starting Y_2O_3/EUROFER powder under fit conditions is then a pressing requirement in order to produce improved ODS EUROFER steels by hipping. We have therefore addressed ourselves to the task of producing the starting Y_2O_3/EUROFER powder under controllable conditions in a research attrition mill. The final product, ready for compaction/HIP processes, consists in the EUROFER 97 steel matrix reinforced with 0.3 wt% of Y_2O_3 particles.

2. Materials

2.1. EUROFER 97 powder

The starting material was EUROFER 97 powder, gas-atomised by Studsvik (Sweden). It was sieved for 1 h in lots of 300 g sequentially using three sieves of sizes 100, 75 and 45 μm. The resulting powder with the finest size, i.e. <45 μm, was selected for the mechanical milling, in order to obtain a better dispersion of the Y_2O_3 particles. The sieved powder was analysed by inductive coupled plasma atomic emission spectroscopy (ICP-AES). Its chemical composition along with that for milled powder is given in Table 1. Fig. 1(a) shows a scanning electron microscopy image of the sieved powder. It can be seen that the particles are spherical and the smallest ones tend to agglomerate.

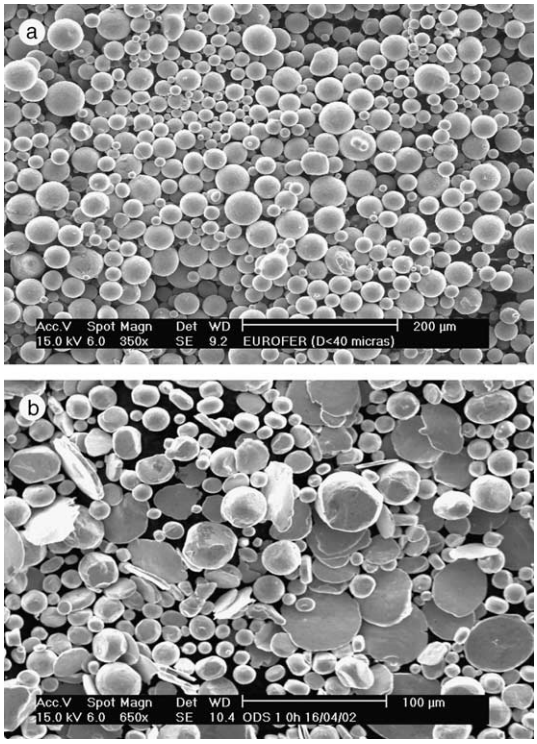

Fig. 1. (a) SEM micrograph of EUROFER 97 powder, particle size <45 μm and (b) SEM image of the Y_2O_3/EUROFER blend after 6 h in a mixer at low rpm.

Table 1
Chemical composition (wt%) of 24 h milled Y_2O_3/EUROFER and <45 μm EUROFER 97 powder along with the specifications for basic EUROFER

Elements	Y_2O_3/EUROFER 24 milled	EUROFER 97 powder size <45 μm	EUROFER 97 specifications
O	0.221 ± 0.011	0.107 ± 0.002	<0.01
N	0.029 ± 0.003	0.014 ± 0.002	0.015–0.045
C	0.136 ± 0.005	0.102 ± 0.002	0.09–0.12
Cr	8.77 ± 0.12	8.88 ± 0.36	8.5–9.5
Mn	0.376 ± 0.007	0.382 ± 0.019	0.20–0.60
Ni	0.080 ± 0.013	0.015 ± 0.001	<0.005
Si	0.032 ± 0.006	0.018 ± 0.002	<0.05
V	0.187 ± 0.009	0.195 ± 0.010	0.15–0.25
W	1.05 ± 0.04	1.130.05	1.0–1.2
Y	0.192 ± 0.006	<0.0005	–

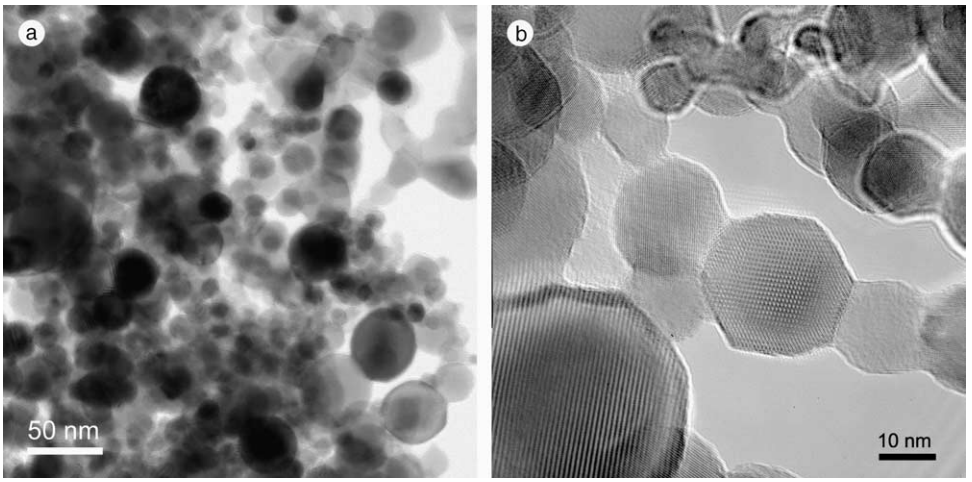

Fig. 2. TEM images of Y_2O_3 powder. (a) Bright field image and (b) HREM image.

2.2. Y_2O_3 powder

Nanometric yttrium oxide (Y_2O_3) of 99.5% purity was provided by PI-KEM (UK) in the form of white powder. The nominal particle size was 15–30 nm. X-ray diffraction measurements were performed on as-received Y_2O_3 powder with an X-Pert Philips diffractometer. The diffraction pattern was adjusted by the Rietveld method with the FULLPROF program [17]. All the peaks of the pattern are consistently indexed with a monoclinic unit cell, space group C2/m. The lattice parameters obtained from the fits are $a = 1.39233(13)$ nm, $b = 0.34944(3)$ nm, $c = 0.86118(8)$ nm and $\beta = 100.228(5)°$.

TEM of the Y_2O_3 powder was carried out with a Philips Tecnai-20 FEG microscope equipped with an energy dispersive X-ray spectrometer operating at 200 kV. Fig. 2 shows the Y_2O_3 particles. The particle size distribution is depicted in Fig. 3. The mean particle size is (20 ± 10) nm.

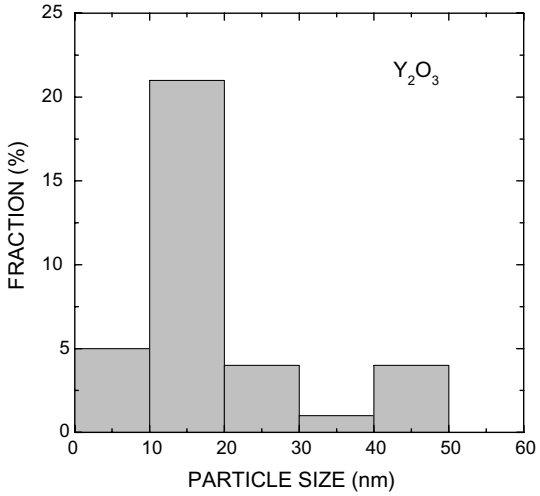

Fig. 3. Particle size distribution of Y_2O_3 powder.

3. Process and optimisation

3.1. Process

The equipment employed is a horizontal attrition mill Simoloyer CM01-2l (Zoz, Germany). Horizontal high-energy ball mills are used for mechanical alloying, high-energy milling and reactive milling in research as well as in industrial applications. This type of mills supplies the highest relative velocity of grinding media (free moving balls), causing an intensive grinding effect, shorter processing times and a lower contamination of the processed powders than the other ball mills. This is because the high kinetic energy process in these mills is due to the collisions of the grinding media instead of shear and friction interactions. During mechanical milling it is impossible to avoid contamination from the grinding media and attritor parts; it is expected that the grinding media cause 95% of the contamination. The materials used inside the attritor chamber are (i) AISI 52100 hardened steel balls of $\varnothing$ 3/16″ for the grinding media, (ii) austenitic steel 1.4301 for the vessel and rotor base and (iii) stellite (Cobalt alloy with W- and Cr-carbides) for the rotor tips.

After contaminating the attritor chamber and the grinding media milling EUROFER 97 powder for several 24 h runs, 150 g of EUROFER 97 powder (size <45 μm) and 0.53 g of Y_2O_3 powder along with 2000 g of steel balls as grinding media were loaded into the attritor for each run. The ball-to-powder ratio was 13:1.

Initially, the EUROFER and Y_2O_3 powders were blended for 6 h in a mixer. However, as Fig. 1(b) shows, this procedure causes the flattening of the EUROFER particles and a certain grade of oxidation. Then, before high-energy milling, blending was carried out in the attritor working at 200 rpm for 2 h, under a pure argon pressurized atmosphere. Next, the mixture was milled for consecutive cycles of 2 h at 800 rpm, separated by rest periods of 30 min running at 100 rpm. During milling, the chamber was pressurized with pure argon and continuously water-cooled to prevent an excessive temperature increase and the oxidation of the powder.

To determine the optimal milling time to produce the Y_2O_3 dispersion, a first batch was produced taking out powder samples after each 2 h cycle. The morphology, X-ray diffraction characteristics and carbon content of the milled powder were checked after every 2 h of milling.

3.2. Morphology of the milled powder

Fig. 4 shows the evolution of the powder morphology during milling. At the beginning, particles agglomerate into flakes with sizes up to 200 μm as Fig. 4(a) reveals. After achieving the maximum size, flakes start to break again, i.e. after around 12 h of milling, see Fig. 4(b). After this point, the extension of the milling time favours the roundness of the resulting particles and lowers their size, as shown in Figs. 4(c) and (d). It should be noticed that the final particle sizes obtained in this first test run are tentatively representative. The venting of the attritor chamber every 2 h of milling to take out a powder sample causes considerable more oxidation of the powder than the case of the continuous milling process. This produces the embrittlement of the particles. Fig. 5 shows the particle of powders continuously milled after 24 and 40 h runs. It is found that the extension of the milling time above 24 h produces no significant changes in the morphology and size of the particles.

3.3. X-ray diffraction line-broadening analyses

Milling induces strong changes in X-ray diffraction-line broadening because of the progressive grain crush and strain accumulation in the crystal lattice. We have applied the method of deconvolution and analysis described in Ref. [18] to determine the respective size and strain contributions to diffraction-line broadening. Fig. 6 shows the characteristic diffraction pattern of the Y_2O_3/EUROFER blend before milling along with the evolution of the full width at half maximum for the (1 1 0) principal reflection ($FWHM_{110}$) with the milling time. Up to milling times around 12 h, the $FWHM_{110}$ value increases steeply due to the decrease of the coherent length and to the strain introduced by plastic deformation. At this stage the powder particles achieve a flattened shape increasing their size.

In addition, the lattice strain is determined applying the 'double-Voigt' line-broadening approach to the principal and secondary reflections, (1 1 0) and (2 0 0), respectively. Fig. 7 shows the mean-square strain along the $\langle 1\,1\,0\rangle$ and $\langle 2\,0\,0\rangle$ directions as a function of milling time. Above 12 h of milling, the fracture of the heavily

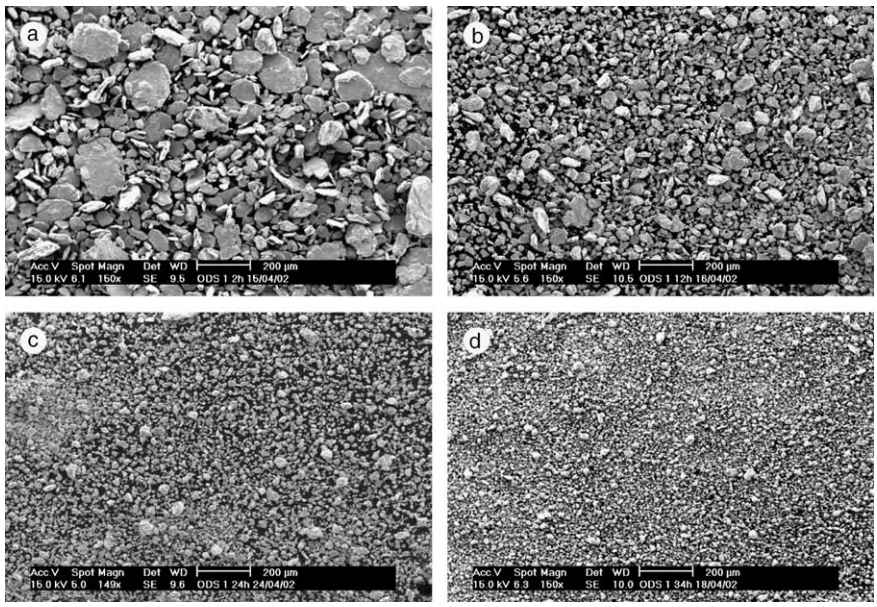

Fig. 4. SEM images of the Y_2O_3 dispersed EUROFER 97 powder. Milled for: (a) 2 h, (b) 12 h, (c) 24 h and (d) 34 h.

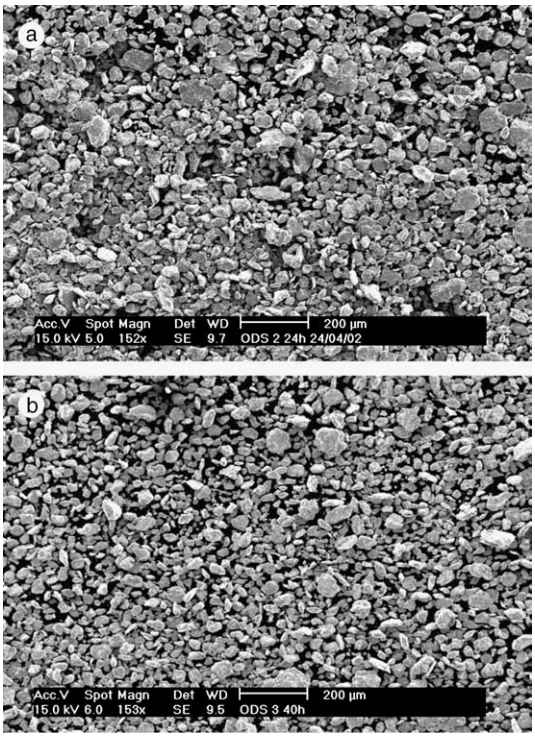

Fig. 5. SEM images of the Y_2O_3 dispersed EUROFER 97 powder after continuous milling. (a) Milled for 24 h and (b) milled for 40 h.

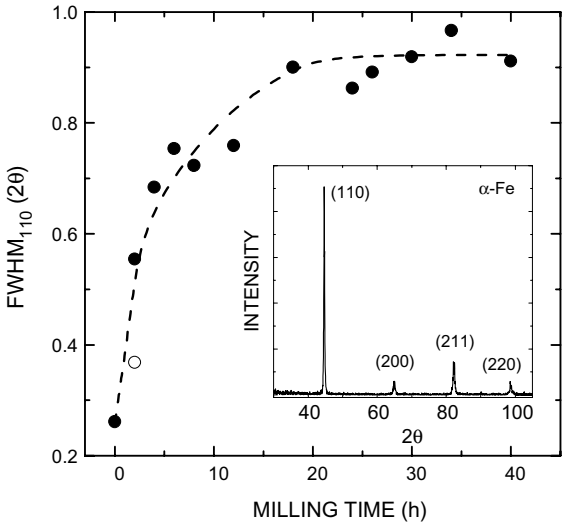

Fig. 6. Evolution of $FWHM_{110}$ with milling time for Y_2O_3/EUROFER powder. The open symbol (○) corresponds to Y_2O_3/EUROFER blended for 2 h in a mixer at low rpm. The inset shows the diffraction pattern of powder before milling.

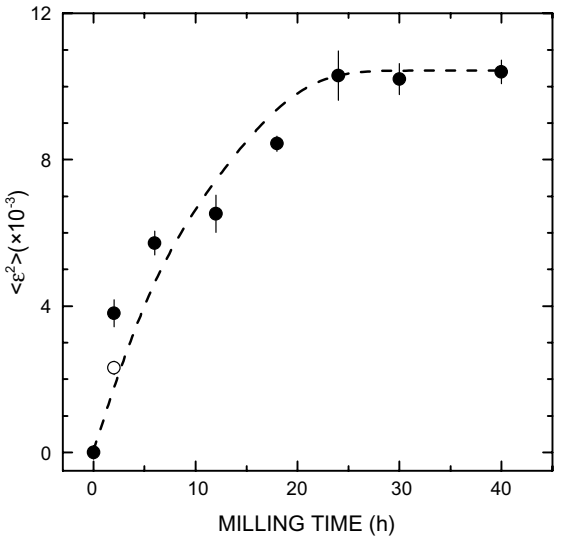

Fig. 7. Mean-square strain as a function of milling time for the Y_2O_3 dispersed EUROFER 97 powder. The open symbol (○) corresponds to ODS blend after 6 h in a mixer at low rpm.

strained particle flakes causes the evolution of the powder morphology to equiaxial shape particles. Now, line broadening becomes insensitive to the fracture and welding processes and tends to a constant value. Under the present milling condition, the maximum strain appears to be achieved after milling for 24 h.

3.4. Composition and TEM analyses of the milled powder

The C, O and N contents in the milled powders were determined by absorption in the IR range using different LECO equipments. Fig. 8 shows the C content as a function of milling time for different batches of milled powders. The C content in the first batch, i.e. batch ODS 1, appears to increase almost linearly with milling time. This effect is attributed to contamination from the grinding media though they were previously contaminated and coated with EUROFER after performing several 24 h runs of milling. The C content in the following batches diminishes significantly being about 0.14 wt% for 24 h runs at 800 rpm starting from batch ODS 3.

ICP-AES analyses were made to check the homogeneity and final composition of the 24 h milled powder. Table 1 shows mean values for the contents of the most relevant elements obtained from analyses for different batches along with the corresponding specified values for basic EUROFER 97. Assuming all the Y content is in the form of Y_2O_3, the resulting Y_2O_3 concentration in the milled powders is 0.24 wt%. This represents a remarkable reduction in relation to the starting Y_2O_3 content of 0.35 wt%. We attribute this reduction to

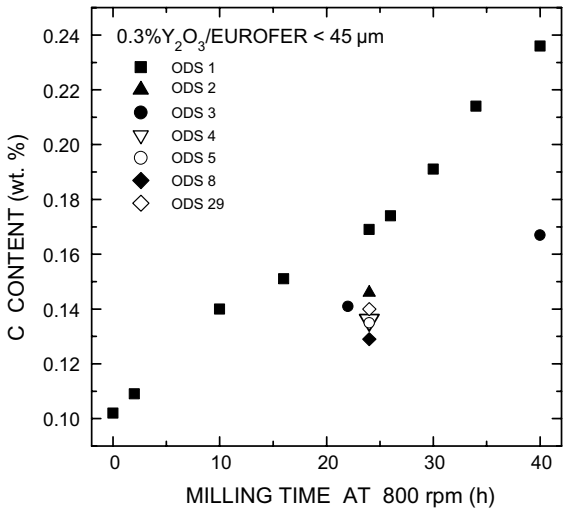

Fig. 8. C content in the Y_2O_3/EUROFER powder as a function of milling time for different batches.

Y_2O_3 loss during the initial purge of the attritor chamber because of the dragging of Y_2O_3 particles by the argon flow.

TEM observations in samples of 24 h milled powder were performed in order to obtain evidence for the Y_2O_3 dispersion in the EUROFER powder. Specimens for TEM were prepared either by ion milling of samples of powder embedded in a solid epoxy resin or by drying a drop of a suspension of powder on a TEM copper grid coated with a thin carbon film. The milled powder was previously crushed using an agate mortar. As Fig. 9(a) shows, there is a high strain accumulated in the samples. The presence of Y_2O_3 nanoparticles dispersed in EUROFER can be seen in the HREM image shown in Fig. 9(b). The observed pattern is consistent with monoclinic Y_2O_3 as revealed by the FFT analyses indicating that the starting monoclinic structure does not change during the milling process. This observation contrasts with the one performed on as-hipped ODS EUROFER where the Y_2O_3 particles are found exhibiting spherical shapes and the more stable cubic phase [15]. Under favourable observation conditions, X-ray energy dispersion evidence for the composition of these particles was attained. The observed Y_2O_3 particle sizes appear to be below 12 nm.

4. Conclusions

The SEM observations indicate that the extension of the milling time above 24 h does not produce apparent changes in the morphology and sizes of the particles. The line-broadening measurements reveal that the strain saturation in the EUROFER particles is attained after 24 h of milling at 800 rpm. This fact indicates that a saturated dispersion of 0.3 wt%Y_2O_3 in EUROFER can be obtained after 24 h of milling following the present procedure. TEM observations reveal the presence of Y_2O_3 nanoparticles dispersed in 24 h milled Y_2O_3/EUROFER powder.

The C contamination from the grinding media increases with milling time. Milling for 24 h at 800 rpm raised the C content up to about 0.14 wt%. This is an acceptable C content for the designed performance of the material that favours the formation of martensite on hipping. The preliminary experiments performed on hipped material, produced from Y_2O_3/EUROFER powders milled for 24 h following the present procedures, have confirmed this point [19]. The O contamination

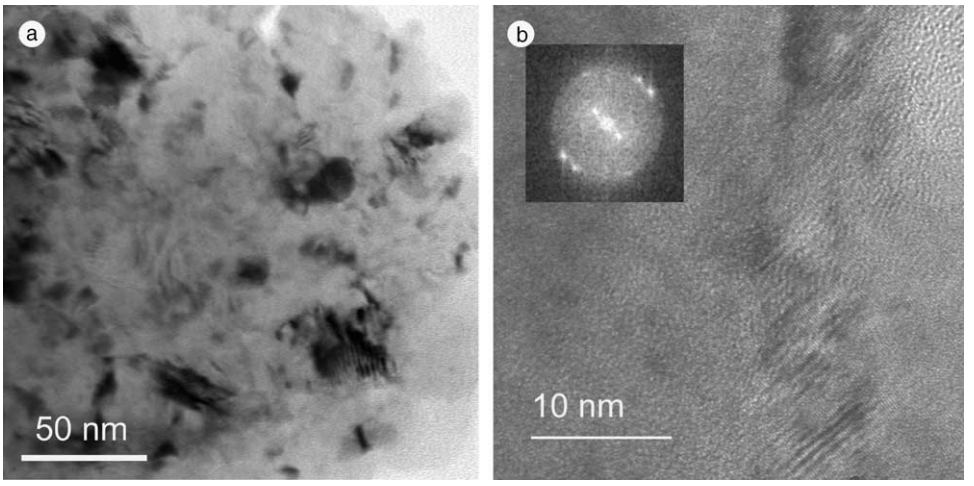

Fig. 9. TEM images of 24 h milled Y_2O_3/EUROFER powder. (a) Bright field image and (b) high resolution image; the inset shows the FFT of an Y_2O_3 particle dispersed in the ferrite matrix.

Table 2
Milling parameter used to disperse Y_2O_3 in EUROFER 97

EUROFER particle size	<45 μm
Y_2O_3 particle size	10–30 nm
EUROFER mass per batch	150.00 g
Y_2O_3 mass per batch	0.53 g
Total powder mass per batch	150.53 g
Total balls mass	2000 g
Grinding media	AISI 52100 balls (∅ 3/16″)
Ratio balls-to-powder	13:1
Attritor full speed	800 rpm
Time at full speed	24 h (12 cycles of 2 h)
Atmosphere	High purity argon
Chamber temperature	24 °C
Number of batches	35
Total mass of Y_2O_3-dispersed EUROFER 97	5.2 kg

after milling is twice the initially determined in the sieved EUROFER powder <45 μm. The contents of the other relevant alloying elements such as Cr, W, V, ... in the 24 h milled powder do not deviate significantly from the specification values for EUROFER. In order to prevent an excessive increase of the C content and the deleterious effect of the O contamination on the impact properties of the hipped material, the milling time was limited to 24 h. Table 2 summarizes the parameters used for the mechanical dispersion of 0.3 wt%Y_2O_3 in EUROFER 97 steel.

Acknowledgements

This research was supported by the Dirección General de Investigación of Spain (Project FTN2000-0959) and the Consejería de Educación de la Comunidad Autónoma de Madrid (Spain) under the auspices of the Financing Program for Strategic Research Groups.

References

[1] R.L. Klueh, D.J. Alexander, E.A. Kenik, J. Nucl. Mater. 227 (1995) 11.
[2] M. Victoria, D. Gavillet, P. Spätig, F. Rezai-Aria, S. Rossmann, J. Nucl. Mater. 233–237 (1996) 326.
[3] A. Kohyama, A. Hishinuma, D.S. Gelles, R.L. Klueh, W. Dietz, K. Ehrlich, J. Nucl. Mater. 233–237 (1996) 138.
[4] A. Hishinuma, A. Kohyama, R.L. Klueh, D.S. Gelles, W. Dietz, K. Ehrlich, J. Nucl. Mater. 258–263 (1998) 193.
[5] B. van der Schaaf, D.S. Gelles, S. Jitsukawa, A. Kimura, R.L. Klueh, A. Möslang, G.R. Odette, J. Nucl. Mater. 283–287 (2000) 52.
[6] E. Daum, U. Fischer, Fusion Eng. Des. 49&50 (2000) 529.
[7] R. Lindau, M. Schirra, Fusion Eng. Des. 58&59 (2001) 781.
[8] R.W. Evans, J. Presto, B. Wilshire, E.A. Little, J. Nucl. Mater. 195 (1992) 24.
[9] S. Ukai, M. Harada, H. Okada, M. Inoue, S. Nomura, S. Shikakura, K. Asabe, T. Nishida, M. Fujiwara, J. Nucl. Mater. 204 (1993) 65.
[10] C. Zankine, C. Prioul, D. François, Mater. Sci. Eng. A 219 (1996) 102.
[11] D.K. Mukhopadhyay, F.H. Froes, D.S. Gelles, J. Nucl. Mater. 258–263 (1998) 1209.
[12] S. Ukai, T. Nishida, T. Okuda, T. Yoshitake, J. Nucl. Mater. 258–263 (1998) 1745.
[13] I.S. Kim, J.D. Hunn, N. Hashimoto, D.L. Larson, P.J. Maziasz, K. Miyahara, E.H. Lee, J. Nucl. Mater. 280 (2000) 264.
[14] S. Revol, S. Launois, R. Baccino, G. Le Marois, B. Rigal, Fusion Eng. Des. 58&59 (2001) 761.
[15] R. Lindau, A. Möslang, M. Schirra, P. Schlossmacher, M. Klimenkov, J. Nucl. Mater. 307–311 (2002) 769.
[16] R. Schaeublin, T. Leguey, P. Spätig, N. Baluc, M. Victoria, J. Nucl. Mater. 307–311 (2002) 778.
[17] J. Rodríguez-Carvajal, Physica B 192 (1993) 55.
[18] D. Balzar, in: R.L. Snyder, H.J. Bunge, J. Fiala (Eds.), Defect Microstructure Analysis from Diffraction, Oxford University, New York, 1999, p. 94.
[19] R. Schaeublin, T. Leguey, N. Nita, R. Bonade, N. Baluc, M. Victoria, in: 11th International Conference on Fusion Reactor Materials, 7–12 December 2003, Kyoto, Japan, submitted.